Surface urban heat island and geospatial indicators: comparative decadal assessment through remote sensing

Ilha de calor de superfície e indicadores geoespaciais: avaliação decadal comparativa por sensoriamento remoto

Iara Nogueira Liguori
Leonardo Marques Monteiro

Abstract

Surface Urban Heat Islands (SUHI) are formed through processes that include decreasing vegetation and increasing materials that are more conductive to heat. To investigate this phenomenon, the objective of this work is to comparatively verify the surface temperature and geospatial indicators to analyze environmental variation in the city of São Paulo, Brazil. The study method is remote sensing, with data from the Landsat 8 satellite over a ten-year timeframe. The variables include land cover, the Normalized Difference Vegetation Index (NDVI), the Normalized Difference Built-up Index (NDBI), and land surface temperature (LST), thereby obtaining the Urban Thermal Field Variation Index (UTFVI) and estimating SUHI formation. The results allowed for the presentation of a progression of variables, highlighting the recurrent formation of SUHI in the central and eastern regions of the city of São Paulo, Brazil. Conversely, the southern and extreme northern districts exhibited the best NDVI indices and low LST values.

Keywords: Urban climate. Remote sensing. Landsat. Surface urban heat island. Land cover. Land surface temperature.

Resumo

A partir dos processos de diminuição da vegetação e aumento de materiais mais condutivos ao calor há a formação de ilhas de calor de superfície (SUHI, do inglês Surface Urban Heat Island). Com o intuito de investigar o fenômeno, o objetivo deste trabalho é verificar comparativamente a temperatura de superfície (LST, do inglês Land Surface Temperature) e indicadores geoespaciais para análise da variação ambiental na cidade de São Paulo, Brasil. O método do estudo é sensoriamento remoto, com dados provenientes do satélite Landsat 8 em um recorte temporal de dez anos. As variáveis são a cobertura do solo, o Índice de Vegetação por Diferença Normalizada (NVDI, do inglês Normalized Difference Vegetation Index), o Índice de Diferença Normalizada de Áreas Construídas (NDBI, do inglês Normalized Difference Built-up Index) e o LST, obtendo em decorrência o Índice de Variação do Campo Térmico Urbano (UTFVI, do inglês Urban Thermal Field Variation Index) e estimando a formação de SUHI. A partir dos resultados apresentou-se uma progressão das variáveis, destacando a formação recorrente de SUHI na região central e zona leste de São Paulo, Brasil. Em contrapartida, os distritos ao sul e extremo norte apresentaram os melhores índices de NDVI e baixos valores de LST.

Palavras-chave: *clima urbano. Sensoriamento remoto. Landsat. Ilha de calor de superfície. Cobertura do solo. Temperatura de superfície terrestre*

[1]Iara Nogueira Liguori
[1]Universidade de São Paulo
São Paulo – SP - Brasil

[2]Leonardo Marques Monteiro
[2]Universidade de São Paulo
São Paulo – SP - Brasil

Recebido em 16/01/24
Aceito em 22/04/24

Introduction

The urbanization processes are closely tied to changes in land use and soil cover, resulting in a radiative alteration among the materials comprising the urban microclimate. This alteration arises from differences in heat radiation between materials, leading to thermal anomalies. Furthermore, the concentration of pollutants, greenhouse gas emissions, and reducing of vegetated areas in urban centers exacerbate climate impact (Oliveira *et al.*, 2020).

The substitution of natural surfaces for materials that conduct heat more effectively leads to the formation of Urban Heat Islands (UHI), characterized by increased temperatures in central and industrial areas compared to the peripheral zones of cities (Gamarra; Corrêa; Targino, 2014).

The investigation of the UHI effect is a widely researched topic within the scientific community, and significant contributions were found in Oke's studies (1973, 1978, 1988), demonstrating the relationship between the size of an urban site and the intensity of its heat island.

The identification of a heat island can be achieved through climatological recording methods, wherein meteorological variables of urban centers and rural areas are compared, resulting in the quantification of the atmospheric heat island (Oliveira *et al.*, 2020). UHI classification includes the analysis of the Urban Canopy Layer (UCL) and the Urban Boundary Layer (UBL) for mesoscale examination (Halder *et al.*, 2022).

More recently, remote sensing methods have been applied involving surface temperature assessment, categorizing UHIs as Surface Urban Heat Islands (SUHI) (Bahi; Mastouri; Radoine, 2020; Fialho, 2012). SUHI analysis can be conducted using various satellites with different sensors and orbital frequencies. For instance, the Terra and Aqua satellites contain the MODIS (Moderate-Resolution Imaging Spectroradiometer) sensor providing a temporal resolution of two images per day, enabling SUHI data daily and nightly. However, its spatial resolution of approximately 1 km limits the analysis of urban microclimates, often being used for evaluating large urbanized areas (Almeida; Teodoro; Gonçalves, 2021).

The Landsat satellites have different sensors. For instance, the Landsat 5 has a TM sensor, the Landsat 7 has an ETM+, the Landsat 8 has a TIRS, and the Landsat 9 has a TIRS 2. They offer an orbital frequency of 16 days with a thermal band resolution ranging from 60 meters to 120 meters depending on the sensor (USGS, 2023). While Landsat satellites provide greater detail of urban microclimates, they do not capture SUHIs at night. Nevertheless, Landsats have a long and uninterrupted observation period since the 1980s, facilitating long-term temporal studies of the same location (Almeida; Teodoro; Gonçalves, 2021; Wulder *et al.*, 2016).

Effat and Hassan (2014) illustrate the SUHI identification process by mapping changes in urban land use and drawing parallels with increased heat islands in Cairo, Egypt. Halder *et al.* (2022) quantify the extent and magnitude of SUHIs using surface thermal data from Landsat and correlating it with land cover. Streutker (2003) observed a rise in surface heat islands in Houston, USA, by compiling the city's radiative temperature maps over 12 years.

Similarly, Farhan, Yang and Lee (2022) analyzed surface temperature data and observed SUHI intensity increasing from 2.47 ºC in 2002 to 3.10 ºC in 2021 in the studied urbanized area. Wang *et al.* (2019) demonstrated through remote sensing how SUHIs can be mitigated by increasing permeable areas in the city.

The systematic collection of data over long periods demonstrates how changes in land use and cover substantially influence rising surface temperatures. Rahman *et al.* (2022), Renard *et al.* (2019), and Zhang, Odeh and Han (2009) conducted qualitative and quantitative sampling over periods exceeding 10 years, utilizing Landsat satellite images and they found a common trend of SUHI increasing alongside urban expansion.

Dorigon and Amorim (2019) identified air temperature patterns in Paranavaí (Paraná, Brazil) and utilized Landsat 8 satellite data to calculate surface characteristics. Monteiro *et al.* (2021) analyzed SUHI presence in 21 metropolitan regions using MODIS sensor data, highlighting the impact of differences in surface temperature, average albedo, and Normalized Difference Vegetation Index. Amorim (2021) combined on-site measurements with Landsat 8 satellite image sensing to develop a methodological framework applicable to small to medium-sized cities.

Gamarra, Corrêa, and Targino (2014) evaluated albedo and surface temperatures obtained from satellite images and correlated them with in-situ air temperatures. Peres *et al.* (2018) studied Rio de Janeiro's SUHIs based on land surface temperature analysis and land use patterns from Landsat 5, Landsat 7, and Landsat 8, noting a significant increase in surface temperature over the years. Ferreira (2021) proposed a methodological approach for analyzing urban surfaces and relating them to surface temperatures provided by Landsat.

Regarding São Paulo city, the studies of Lombardo (1985) and Barros and Lombardo (2016) quantified temperature differences between central and peripheral areas up to 10 ºC. Ferreira (2019) and Ferreira and Duarte (2019) examined the relationship between vegetation, surface temperature, and urban morphology in the metropolitan region of São Paulo using MODIS data, demonstrating that more urbanized areas have higher daytime and nighttime surface temperatures than less urbanized areas.

For that matter, the objective of this work is to compare the surface temperature and geospatial indicators to analyze the environmental variation and the occurrence of SUHI in the city of São Paulo, Brazil, using data collected from the Landsat 8 satellite over ten years.

Method

The method is divided into four stages:

(a) identification of the urbanized area;

(b) collection of data from the Landsat 8 satellite;

(c) image composition and processing; and

(d) data analysis and interpretation.

Identification of the urbanized area

The object of study is the city of São Paulo - SP, Brazil, latitude 23.5º S, and longitude 46.6º W, located in Bioclimatic Zone 3 (ABNT, 2005), at an altitude of approximately 750 meters (Figure 1). The urban climate is humid subtropical, classified as Cwa by Köppen-Geiger, marked by seasonality, with moderately hot, rainy summers and dry cold winters.

Data collection

The data were collected from the Landsat 8 OLI/TIRS satellite, which provides freely available images through Science For a Changing World (USGS).

As a selection criterion, only cloud-free atmospheric images recorded between 2013 and 2023 were utilized, encompassing a total of 10 years. This analysis period covers the entire operational cycle of the Landsat 8 OLI/TIRS satellite, which has been providing geospatial images since 2013.

A subsequent examination revealed that the majority of cloud-free images were captured during August and September, which are characterized by a predominantly dry climate. This choice of timeframe establishes a consistent temporal baseline and mitigates seasonal variability, facilitating the comparison and interpretation of results.

Figure 1 **- Location of São Paulo - SP, Brazil, with RGB composition and division of districts. Data collected from Landsat 8, corresponding to 09/02/2022, a composition made in Qgis software**

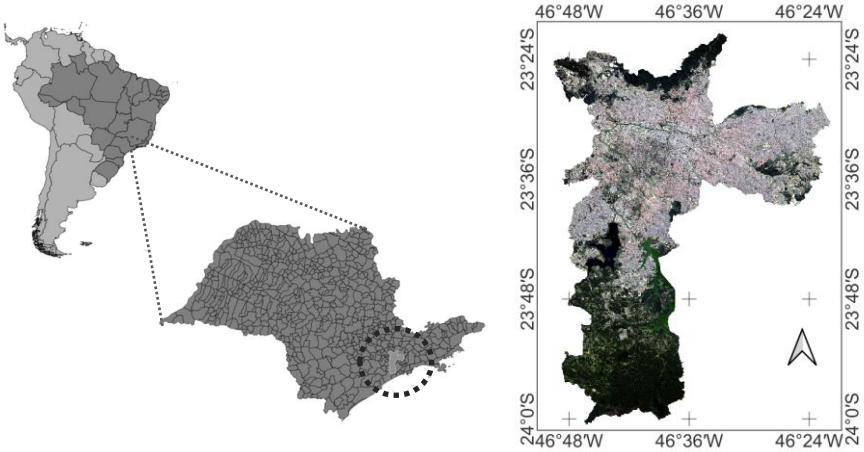

In Table 1, data gaps exist for the years 2014, 2016, and 2020 due to the absence of suitable images meeting the established criteria.

To visualize the results, compositions of geospatial indices will be presented for 2013, the initial year of data collection, for 2017, selected due to its high surface temperature values and representing the midpoint of the analyzed period, and for 2023, the most recent year. Statistical results for all years will be systematized and graphically presented.

The maps were generated using the QGIS software, utilizing bands 2, 3, and 4 for the RGB (red, green, and blue) color composition. Bands 5 and 6 were employed to create the Normalized Difference Built-Up Index (NDBI) map, bands 4 and 5 for the Normalized Difference Vegetation Index (NDVI) map, and band 10 for Land Surface Temperature (LST) calculation (Table 2).

The data are derived from Level 1 images and calibrated with basic adjustment parameters for final use (USGS, 2024). However, Level 2 images contain refined data, which helps reduce possible distortions caused by electromagnetic radiation. It is important to note that when utilizing Level 1 images, atmospheric correction is necessary to improve temporal analysis of the images. In this study, to streamline the process and introduce the Land Surface Temperature Estimation plugin (Ndossi; Avdan, 2016), we opted to utilize Level 1 image data when analyzing orbital images over time.

Image composition and processing

The analyzed variables include land cover from post-processing of the RGB images, as well as NDBI, NDVI, and LST. Then, maps of the Urban Thermal Field Variance Index (UTFVI) can be generated, and SUHI can be measured.

The following flowchart (Figure 2) outlines the image composition processes using bands from the Landsat 8 satellite.

Table 1 – **Selected days based on the established criteria**

Year	Date
2013	September 01
2015	September 23
2017	September 12
2018	August 30
2019	August 17
2021	August 22
2022	September 02
2023	September 13

Table 2 – **Bands used**

Bands	Use	Spectral Range	Resolution
Band 2	Blue	0.450 - 0.51 µm	30 m
Band 3	Green	0.53 - 0.59 µm	30 m
Band 4	Red	0.64 - 0.67 µm	30 m
Band 5	Near-Infrared (NIR)	0.85 - 0.88 µm	30 m
Band 6	Short-wave infrared (SWIR 1)	1.57 - 1.65 µm	30 m
Band 10	Thermal Infrared Sensor (TIRS)	10.6 - 11.19 µm	100 m

Source: adapted data provided by United States Geological Survey (2023).

Figure 2 - **Flowchart of image composition stages**

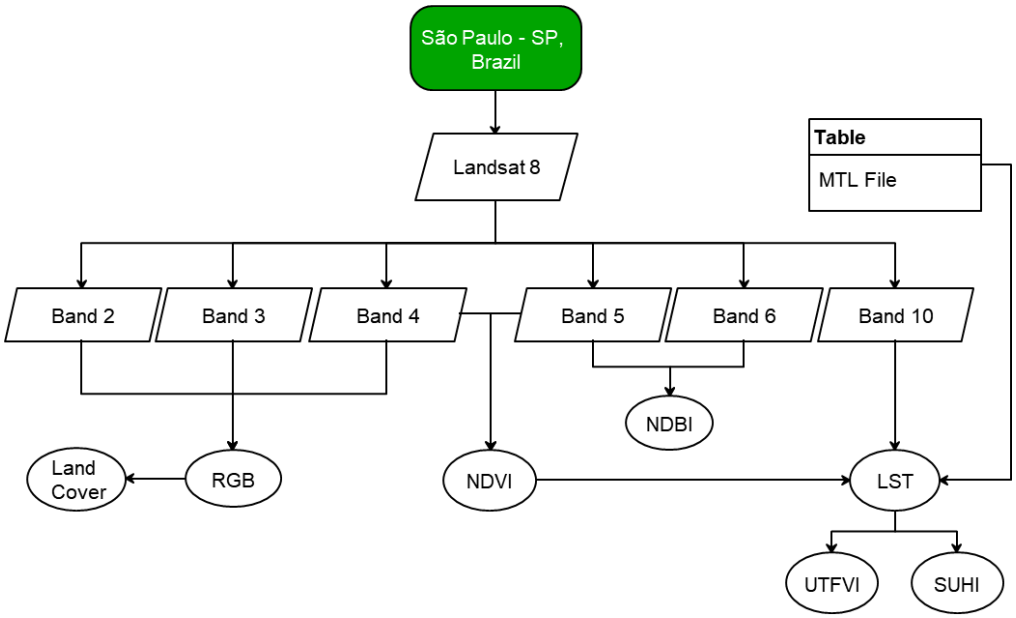

Source: developed by the authors, method from Oliveira and Giacaglia (2018).

Land cover

Land cover refers to the physical aspects of the surface and is calculated from the spectral signature of the materials within the scene (Ribeiro, 2017). Each surface exhibits distinct patterns of reflection, absorption, or emission of electromagnetic energy. Through band combination, a multispectral composition is created, enabling the identification of various classes and highlighting areas with potentially higher surface temperatures (Oliveira *et al.*, 2020).

The intermediary step in this process involves generating an RGB image, achieved by combining bands 4 (red), 3 (green), and 2 (blue). Subsequently, the image can be classified, and Regions of Interest (ROIs) can be delineated.

The Semi-Automatic Classification Plugin (Congedo, 2021), installed at QGIS software, was used to construct the land cover maps. Four classes of São Paulo were identified:

(a) urbanized area;

(b) exposed soil;

(c) vegetation; and

(d) water.

These classes were segmented into training polygons for algorithmic processing and the maps were generated.

Normalized Difference Built-up Area Index (NDBI)

NDBI is essential for comprehending the urbanization process and indicates the density of built-up areas within a given urban landscape (Halder *et al.*, 2022). This index is derived from the reflectance characteristics of the short-wave infrared (SWIR), which typically exhibits higher values compared to the near-infrared (NIR) (Zha; Gao; Ni, 2003).

The index is represented in a range from -1 to +1, wherein values nearing +1 indicate high urban density, while areas devoid of urban development are represented by values near -1 (Zha; Gao; Ni, 2003). Intermediate values typically denote areas with mixed land cover, where urbanized regions exhibit an NDBI greater than zero, contrasting with other land covers registering values less than zero (Wang *et al.*, 2023).

NDBI is calculated by the ratio between the shortwave infrared (SWIR1) and near-infrared (NIR), as depicted in Equation 1.

$$NDBI = \frac{SWIR1-NIR}{SWIR1+NIR} \quad \text{Eq. 1}$$

Where:

NDBI is the Normalized Difference Built-up Area Index;

SWIR1 is the Short-wave infrared, corresponding to band 6 for Landsat 8; and

NIR is the Near-Infrared, equivalent to band 5 for Landsat 8.

Normalized Difference Vegetation Index (NDVI)

NDVI values serve to evaluate changes in land cover by monitoring changes in vegetation cover and identification of the urbanization process (Rodriguez-Galiano *et al.*, 2012; Voogt; Oke, 2003; Silva *et al.*, 2020).

The index is computed from the spectral reflectance disparities between the red (RED) and near-infrared (NIR) bands (Equation 2) (Kshetri, 2018). Besides evaluating vegetation quality within the study area, NDVI also serves as an intermediary step in Land Surface Temperature (LST) computation.

The NDVI values are depicted on a scale ranging from -1 to +1. Negative values signify the existence of water bodies, while those near zero indicate urbanized areas and exposed soil. Positive values signify the presence of vegetation, with values closer to +1 signifying higher quality and density of vegetation within the study area.

$$NDVI = \frac{NIR-RED}{NIR+RED} \quad \text{Eq. 2}$$

Where:

NDVI is the Normalized Difference Vegetation Index;

NIR is the Near-Infrared, equivalent to band 5 for Landsat 8; and

RED is the Red band, corresponding to band 4 for Landsat 8.

Land Surface Temperature (LST)

LST denotes the radiative variance among surfaces and enables the measurement of temperature disparities between analyzed areas, essential for computing UTFVI and SUHI.

The outcomes are derived from the Land Surface Temperature Estimation plugin (Ndossi; Avdan, 2016), involving five processing steps. Intermediate processes include estimating the radiance, brightness, and emissivity of the Earth's surface (Figure 3).

Step 1: radiance

Radiance is determined by the electromagnetic energy received by the sensor. This stage involves converting Digital Numbers (DN) data into a representation of spectral radiance at the Top-of-Atmosphere (TOA) (Ndossi; Avdan, 2016). The plugin automatically executes this process, requiring input of band 10 and the MTL file.

Figure 3 - **Flowchart of LST composition stages**

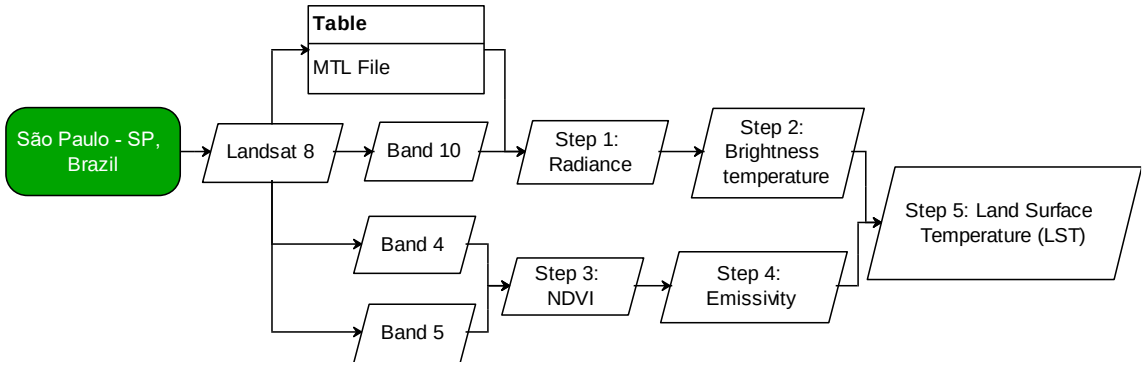

Source: developed by the authors, method from Oliveira and Giacaglia (2018).

Step 2: brightness temperature

The resulting radiance band is utilized to calculate brightness temperature. This step computes the temperature necessary for a black body to emit the same radiation as the area under analysis (Ndossi; Avdan, 2016).

Step 3: NDVI

As previously described, NDVI is computed from bands 4 and 5 using Equation 2.

Step 4: emissivity

Emissivity varies with wavelength and it is derived from the thermophysical properties of materials. It is determined from the ratio between emitted radiance and blackbody emission, extracted from the NDVI raster (Ndossi; Avdan, 2016).

Step 5: land surface temperature

The final step in the process is calculating surface temperature, derived from combining brightness and emissivity temperature rasters. The resultant product is expressed in Celsius (°C) and visualized on maps and statistical graphs.

Urban Thermal Field Variation Index (UTFVI)

The UTFVI is used to quantitatively assess the surface temperature of each pixel in the urbanized area relative to the average LST in order to obtain a classification of environmental quality (García; Díaz, 2023). It is calculated by the ratio of the pixel's LST and the average LST, where the average LST is obtained from statistical analyses of the raster (Equation 3).

$$UTFVI = \frac{LST_{pixel} - LST_{average}}{LST_{average}} \quad \text{Eq. 3}$$

Where:

UTFVI is the Urban Thermal Field Variation Index;

LSTpixel is the Land Surface Temperature of the pixel; and

LSTaverage is the Average Land Surface Temperature.

UTFVI values can be classified into six levels of ecological assessment and are related to the presence of SUHI and its impact on the environmental quality of the urban climate (Table 3) (Halder *et al.*, 2022).

Table 3 – **Scale of UTFVI and level of ecological variation**

UTFVI	Urban thermal island phenomenon	Ecological evaluation index
< 0	None	Excellent
0–0.005	Weak	Good
0.005–0.010	Medium	Normal
0.010–0.015	Strong	Poor
0.015–0.020	Strongest	Worst
> 0.020	Strongest	Worst

Source: Halder *et al*. (2022).

Surface Urban Heat Island (SUHI)

The surface urban heat island is assessed based on pixels selected within the scope of the analyzed urban site, irrespective of the urban or rural context (Faisal *et al.*, 2021). Consequently, the urban thermal balance is obtained from the interplay between the pixel's Land Surface Temperature (LST), the mean LST, and the evaluation of the standard deviation (Halder *et al.*, 2022) (Equation 4).

$$SUHI = \frac{LST_{pixel} - LST_{average}}{SD} \quad \text{Eq. 4}$$

Where:

SUHI is the Surface Urban Heat Island;

LST_{pixel} is the Land Surface Temperature of the pixel;

$LST_{average}$ is the Average Land Surface Temperature; and

SD is the Standard Deviation.

Data analysis and interpretation

After data acquisition and processing, the images were colored to facilitate result interpretation. Additionally, the statistical data were graphically systematized.

Results

Land cover

By analyzing land cover, it is possible to identify areas of interest in the dynamics of the urban environment, with a spatial distribution of classes and potential areas with higher surface temperature values (Barros; Lombardo, 2016).

The land cover analysis is depicted in Figure 4, comprising two maps of São Paulo: the first corresponds to 2013, and the second to 2023. Both maps are color-coded, with red representing urbanized areas, yellow representing exposed soil, green illustrating vegetated areas, and blue indicating water bodies.

Upon examining the images, a noticeable urban concentration is observed in central areas, with remaining vegetation located to the south and far north of the city. Water bodies such as the Billings and Guarapiranga reservoirs are prominently featured to the south of the urbanized area, alongside the environmental conservation area encompassing the Parelheiros, Grajaú, and Marsilac districts.

A comparison between the 2013 and 2023 maps reveals an expansion of the urbanized area (Magalhães; Toscano; Bergamaschi, 2013), accompanied by a reduction in exposed soil primarily to the south and far north of the urban site. Furthermore, it is evident in both years that parks and conservation units are being preserved.

In Figure 5, the classes are correlated in km², allowing a more precise visualization of the urban land distribution. When analyzing the data, it is possible to notice an increase in urbanization, since for the year 2013 the area was 750.9 km², or 49.17%, while in the following period, the area increased to 808.9 km², or 52.97%. The difference is compensated by the reduction in exposed soil, as in 2013 there was an area of 143.9 km², representing 9.42% of the urban area, while in 2023 the area decreased to 77.3 km² or 5.06%. For the vegetation and water classes, no significant changes were observed when comparing the years.

Normalized Difference Built-up Area Index (NDBI)

NDBI allows the identification of urbanized areas with a greater degree of precision and objectivity (Zha; Gao; Ni, 2003), establishing a strong positive correlation with LST (Zhang; Odeh; Han, 2009). Figure 6 illustrates the NDBI outcomes for São Paulo. The maps display a gradient of colors, with dark blue indicating the lowest NDBI values, corresponding to areas with low built density, while yellow signifies regions with high NDBI values and heightened urban occupation.

Figure 4 - **Land Cover images corresponding to the years 2013 and 2023, respectively**

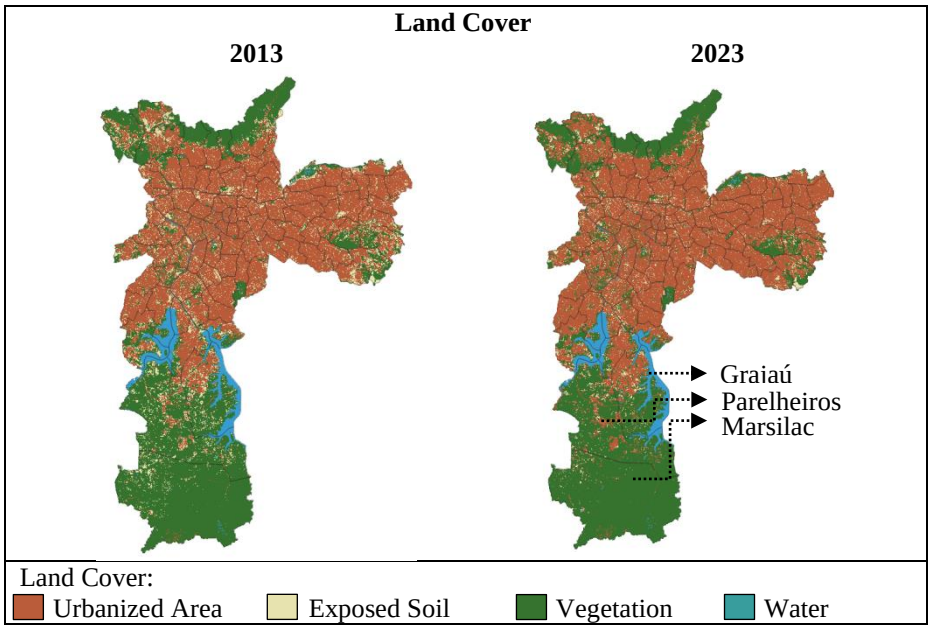

Figure 5 - **Land cover classification in km²**

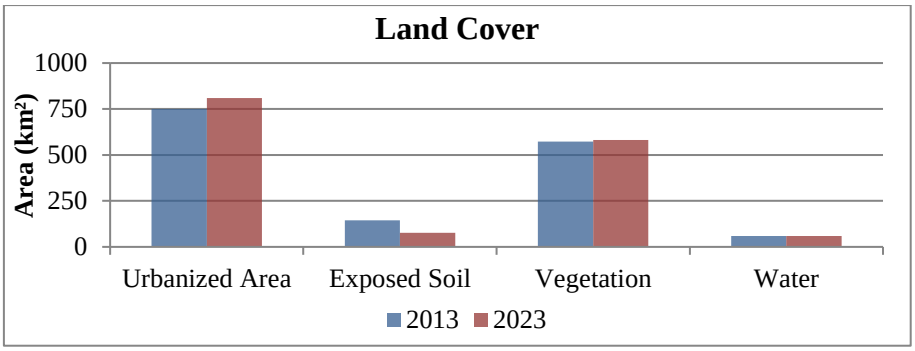

Figure 6 - **NDBI Maps for the Years 2013, 2017, and 2023**

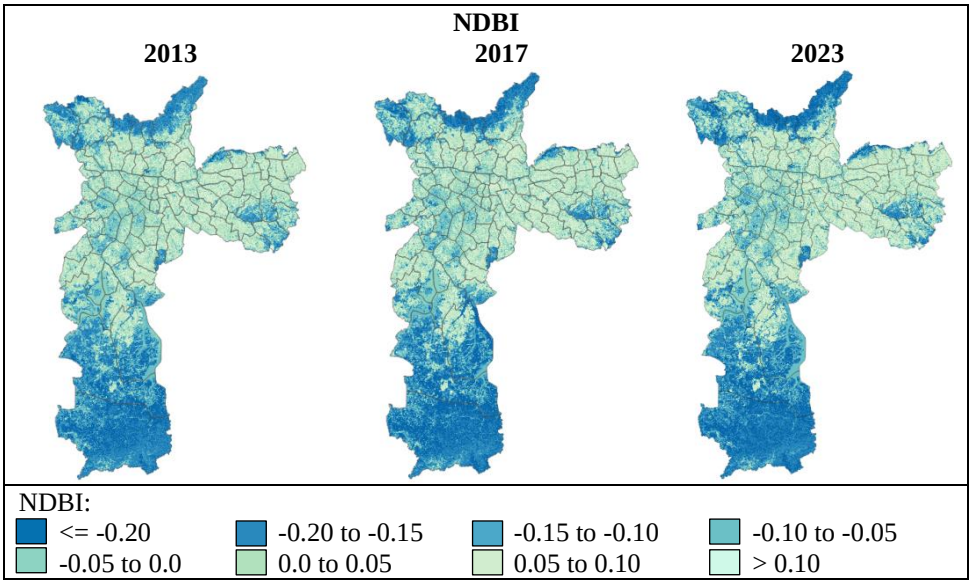

Comparing the maps, it becomes evident that the index predominates in the central and eastern regions, showing minimal variability over the years. The minimum values, below -0.15 and represented in dark blue,

correspond to places with a predominance of vegetation, i.e. the south and far north of São Paulo. The moderate intermediate values, -0.15 to 0.0, are spaced out and correspond to places with low urban density and mixed cover. Finally, the highest NDBI values, greater than zero and represented in yellow, can be seen in the center and east of the city.

A similarity is observed when comparing the maximum, minimum, and average NDBI values for the years 2013 to 2023 (Figure 7). The maximum urban density value corresponds to the years 2013 and 2015, both presenting a value of 0.5. The minimum NDBI value was recorded in 2021, with a value of -0.57. The average NDBI remains consistent across all years, at -0.05. The standard deviation fluctuates between 0.09 and 0.11.

Normalized Difference Vegetation Index (NDVI)

NDVI analysis shows the spatial, temporal, and qualitative variations of urban vegetation, representing an important indicator of land surface temperature (Ferreira, 2019).

The density and quality of vegetated areas are depicted in Figure 8, showing NDVI maps for the years 2013, 2017, and 2023. The maps are represented on a color scale, where green indicates higher NDVI values, corresponding to greater vegetated area density, while brown represents areas with higher urban density or water bodies, signifying lower NDVI values.

Figure 7 - **Statistical Results of Standard Deviation and Mean, Maximum, and Minimum NDBI for the Period Under Analysis**

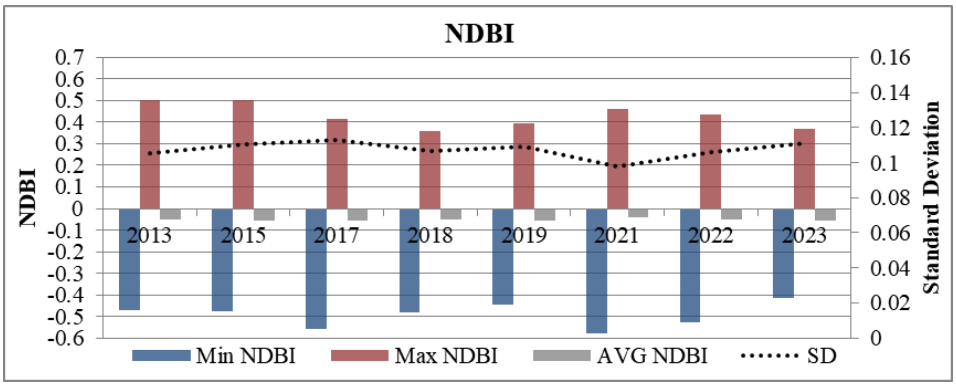

Figure 8 - **NDVI Maps for the years 2013, 2017, and 2023**

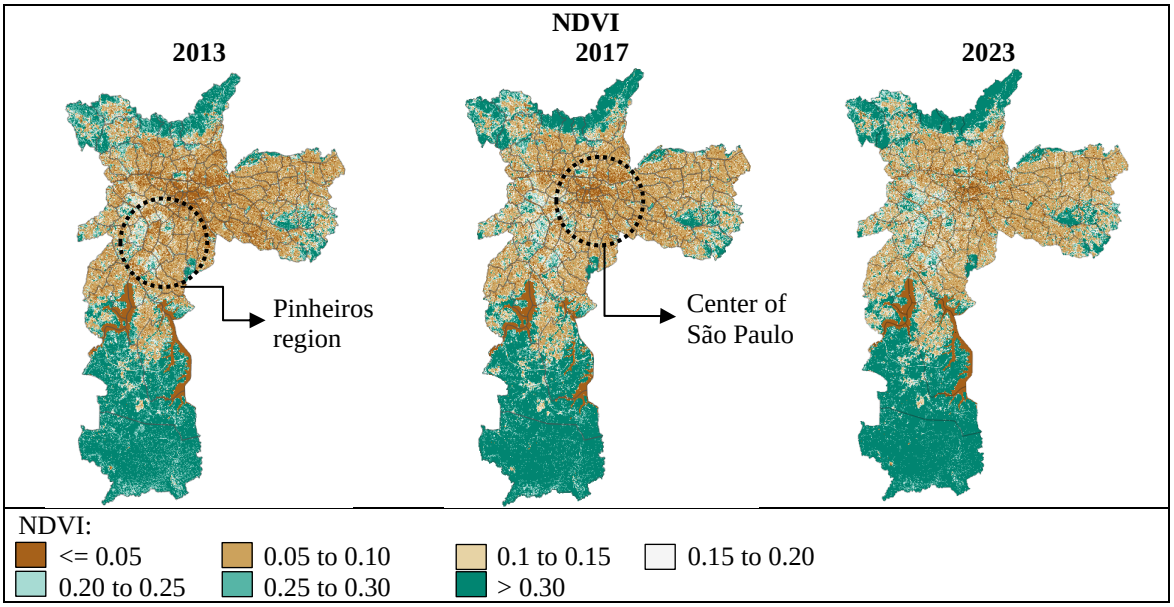

The NDBI results indicate that urban density predominates in the central and eastern regions, followed by vegetated areas in the south and far north. As a consequence, the highest NDVI values are found in these areas and show results greater than 0.25. The lowest NDVI values, below 0.05, correspond to the water bodies. The

moderate intermediate, 0.15 to 0.25, is seen in the Pinheiros region, which is known to be the most wooded locality in the urban area. Lastly, the city center stands out in the high intermediate range, 0.05 to 0.15. Apart from the increase in urbanization, demonstrated by the land cover results, it was not possible to ascertain a qualitative temporal variation (Ferreira, 2019).

The statistical analysis of the index (Figure 9) corroborates the previous results, where the maximum NDVI is similar for all years, with values close to 0.6. The minimum NDVI is also consistent throughout the period, at -0.35. The average NDVI corresponds to a value of 0.2, with the lowest index result occurring in the year 2021. The standard deviation shows values ranging from 0.12 to 0.14.

The NDVI results are similar to those demonstrated by Ferreira (2019) and Ferreira and Duarte (2019) since the authors applied the index to the São Paulo Metropolitan Region and confirmed the correlations found between NDVI values and the urbanized area, indicating the role of vegetation in attenuating surface temperatures. The high NDVI values are also confirmed by Monteiro *et al.* (2021), who correlated the index for the main Brazilian capitals and found a ΔNDVI of -0.22 in São Paulo.

Land Surface Temperature (LST)

Surface temperatures exhibit high spatial and temporal variability, consistent with the moment of imaging, providing information inherent to the moment of data collection, and highlighting dynamism when comparing different periods (Amorim, 2021). The LST maps (Figure 10) are represented on a color scale, where shades of blue characterize minimum values, and shades of red depict maximum values of surface temperature.

Upon analyzing the maps, it is possible to observe a high thermal variation due to urban concentration, where areas with high NDBI values and low NDVI values showed higher surface temperatures. Among the maps presented, the 2013 year stood out with the lowest LST values, with densely vegetated areas showing values close to 26 ºC and densely populated areas showing values between 30 ºC and 34 ºC. The year 2017 stands out with the highest LST values, with temperatures exceeding 36 ºC recurring. The result is due to the weather conditions at the time of imaging and indicates the performance of the urban site in high temperature situations. Finally, the 2023 year is intermediate between the maps presented, with maximum temperature pixels between 34 ºC and 36 ºC.

Figure 9 - **Statistical results of standard deviation and average, maximum, and minimum NDVI for the period under analysis**

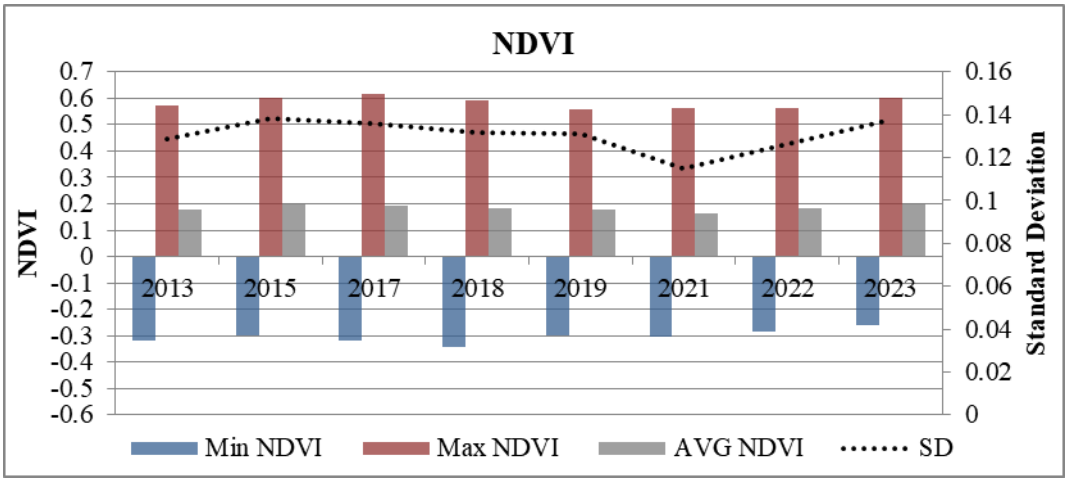

Figure 10 - **LST maps for 2012, 2017, and 2023**

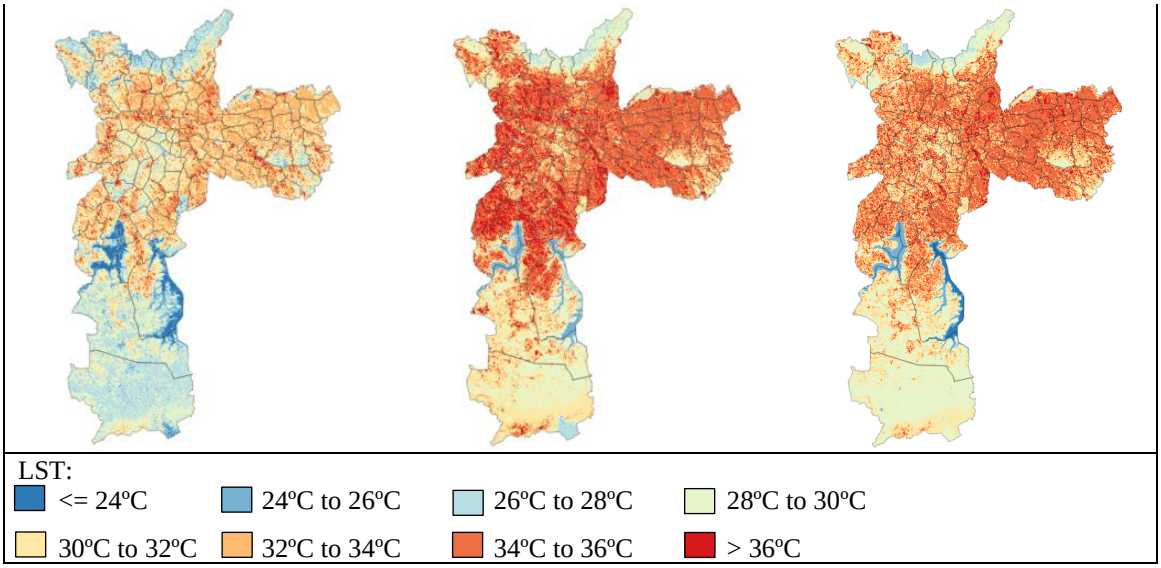

The difference in temperature between the densely populated urban areas and the more predominantly vegetated areas was approximately 6 ºC. In this sense, as demonstrated in the work by Ferreira (2019), although the urbanized area shows warming trends, it is not possible to measure a homogeneous LST, highlighting the morphological differences of the urban surface.

The statistical analysis of the data (Figure 11) reveals that the years 2013, 2015, 2017, and 2023 exhibited similar maximum surface temperatures, close to 45 °C. The years 2018, 2019, 2021, and 2022 also exhibit correlated maximum temperatures, at approximately 40 °C. The minimum LST showed greater amplitude, with a value of 16.1 °C in 2019 and the minimum surface temperature reaching 23.8 °C in 2017. The average temperature also showed a fluctuation of approximately 9 °C, with lower values observed in 2019 and maximums corresponding to 2015. The standard deviation follows the previous results.

Urban Thermal Field Variance Index (UTFVI)

The UTFVI characterizes the quality of urban ecology and is an important indicator of the heat island effect (Halder; Haghbin; Farooque, 2021). In Figure 12, the index is shown on a color scale in corresponding maps for the entire analysis period, with red areas indicating the higher values.

The UTFVI values reiterate the previous results. It is noted that the districts to the south express good urban quality since the UTFVI values are lower than zero. The worst index results, exceeding 0.20, indicating the possibility of SUHI formation and are recurrent in the center and east zone. The central regions near Pinheiros, as shown by the NDVI results, exhibit good urban quality, with pixels mostly between 0.0 and 0.10.

The UTFVI maps for 2013, 2017, and 2023, as well as the average UTFVI, show significant similarities, with a notable repetition in the values, indicating low urban variability over the analyzed period.

Table 4 presents the minimum and maximum UTFVI data for the entire period under analysis. The minimum UTFVI shows little variability over the years, with 2015 having the lowest value, -0.5, followed by 2013, 2019 to 2023 with a value of -0.4, and finally 2017 and 2018 with a minimum UTFVI of -0.3. The maximum UTFVI shows greater oscillation, with the index in 2023 being 0.49, and in 2019 the value is 1.01. When correlating the values, there is no significant change in UTFVI over the analyzed period. The average UTFVI and the standard deviation showed values in exponential notation and were therefore not computed.

The values' averages were calculated based on the UTFVI maps, and these were sectorized by district of São Paulo; the results are shown in Figure 13.

Figure 11 - **Statistical results of standard deviation and average, maximum, and minimum LST for the period under analysis**

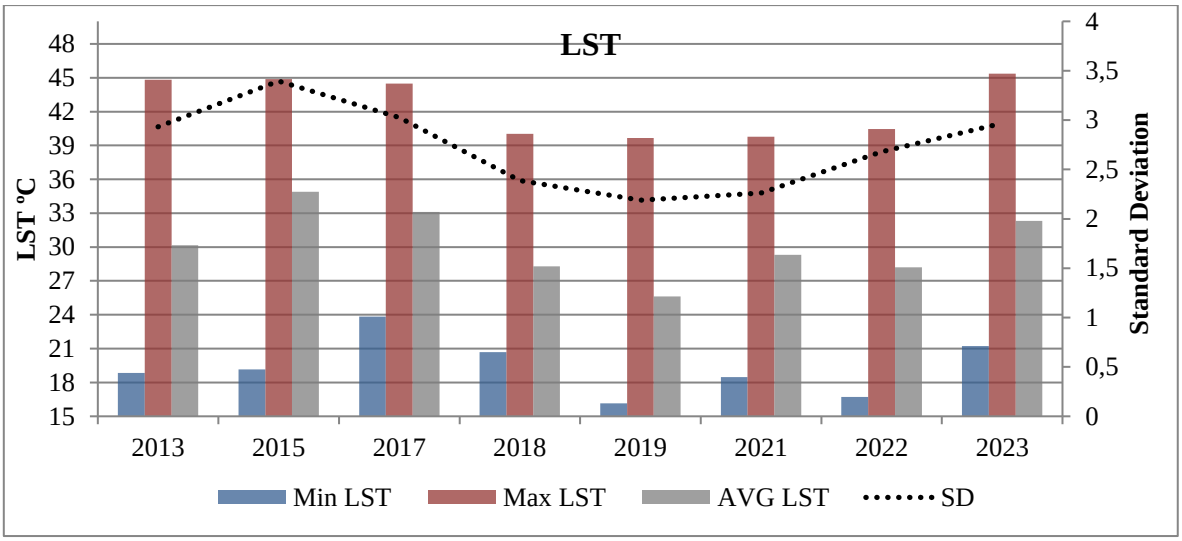

Figure 12 - **UTFVI for 2012, 2017, and 2023 and UTFVI average**

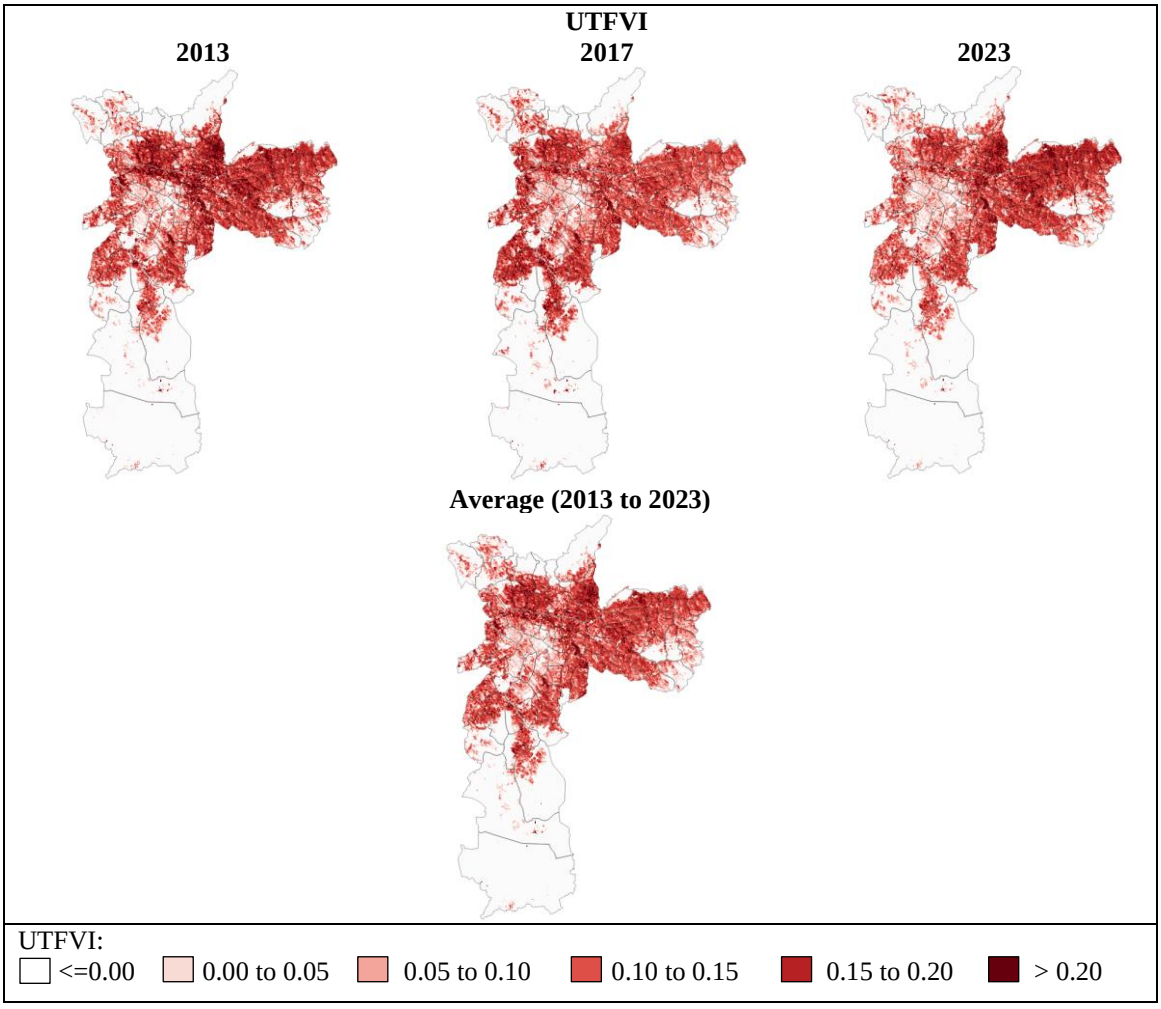

Table 4 - **Maximum and minimum UTFVI values for the entire period**

UFTVI

Years	2013	2015	2017	2018	2019	2021	2022	2023
Min	-0.4	-0.5	-0.3	-0.3	-0.4	-0.4	-0.4	-0.4
Max	0.76	0.7	0.74	0.93	1.01	0.52	0.61	0.49

Figure 13 – **Maps of average sectorized UTFVI by district of São Paulo, Brazil**

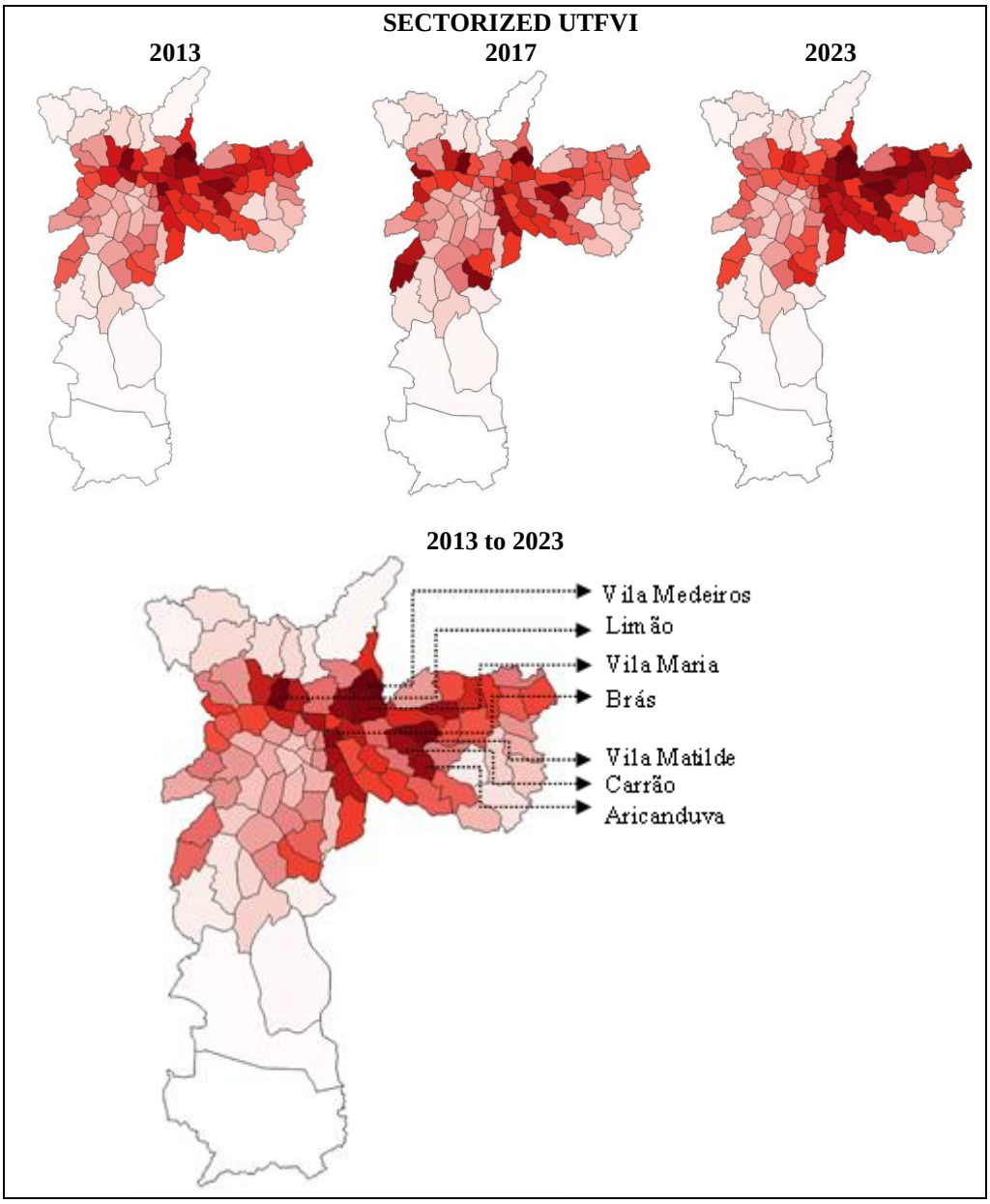

When comparing the results from 2013 to 2023, there is a decrease in the index in the eastern part of the city, with an increase in districts with poor urban quality. After analyzing the map, it becomes evident that the central districts of the city, especially Vila Medeiros, Limão, Vila Maria, and Brás are those with the worse indices, followed by the eastern zone, with emphasis on the districts of Vila Matilde, Carrão, and Aricanduva.

Surface Urban Heat Island (SUHI)

The SUHI maps are presented in Figure 14, and similar to the previous maps, there is a color scale. Areas represented in red are those with a high occurrence of surface urban heat islands, while those in blue show no incidence of the effect.

The analysis of the maps indicates a repetition of the episodes demonstrated by the UFTVI, as the SUHI maps reveal the locations where the urbanized area is most affected by urban concentration, as evidenced by the NDBI. The SUHI maps for 2013, 2017, and 2023 and average SUHI maps show little variation. Nevertheless, the 2013 map shows a higher recurrence of pixels higher than 2.0 in the central region, indicating the occurrence of the phenomenon. In 2023, the SUHIs shifted towards the eastern part of São Paulo.

Figure 14 - **SUHI for 2012, 2017, and 2023 and SUHI average**

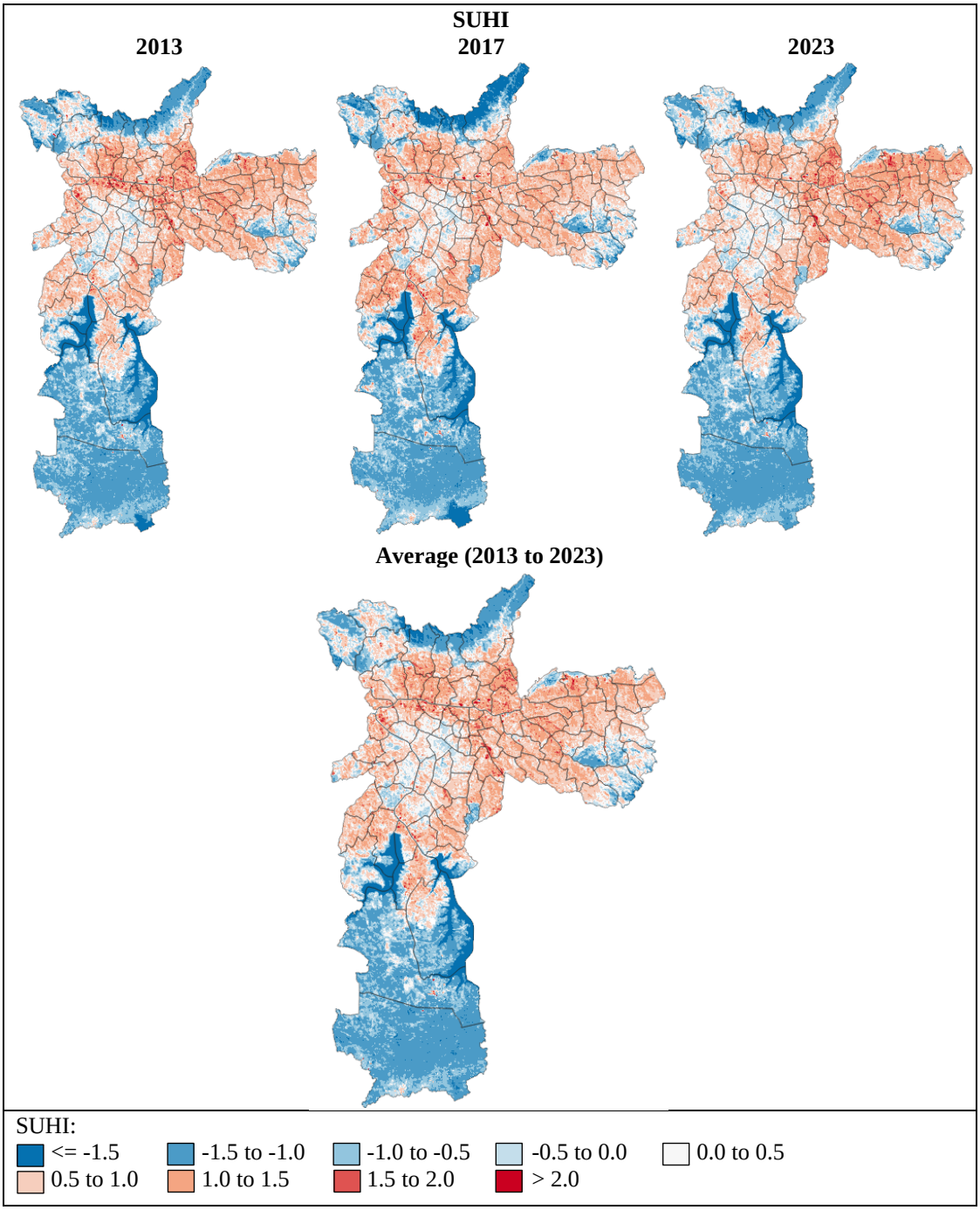

The minimum and maximum SUHI data for the period under analysis are shown in Table 5. When analyzing the results, it is evident that, like the UTFVI, the minimum values show less variation, with 2015 showing the

lowest result, -3.52. There is more variation in the maximum SUHI indexes, with the highest value corresponding to 2019, 7.34, and in 2023, 3.59.

The previous findings are reinforced when correlating SUHI with urban districts, where areas close to urban central axes have a higher incidence of surface heat islands, represented in red (Figure 15). Districts in dark blue correspond to those with conservation units and showed better NDVI values.

In contrast to districts with high UFTVI values, some locations in São Paulo feature tree-lined streets, parks, and good urban quality, such as the districts of Jardim Paulista, Pinheiros, Itaim Bibi, and Morumbi. These districts exhibit low surface heat island indexes and are illustrated by the light blue color on the map.

Table 5 - **Maximum and minimum SUHI values for the entire period**

	SUHI							
Years	**2013**	**2015**	**2017**	**2018**	**2019**	**2021**	**2022**	**2023**
Min	-2.77	-3.52	-2.47	-2.46	-2.95	-3.25	-3.11	-2.76
Max	5.22	5.01	5.40	7.09	7.34	4.25	4.27	3.59

Figure 15 - **Maps of average sectorized SUHI by district of São Paulo, Brazil**

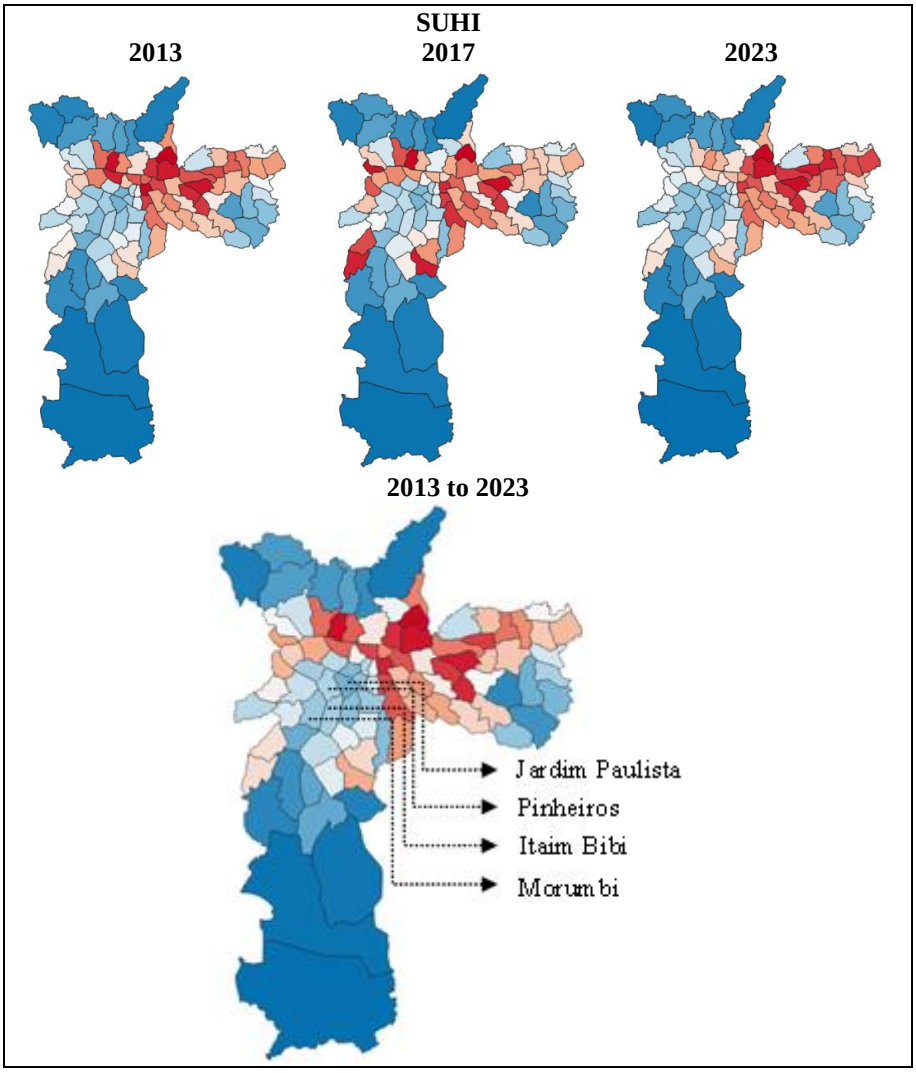

The presence of SUHIs in São Paulo is supported by Oliveira *et al.* (2020), Monteiro *et al.* (2021) and Ferreira (2019). Furthermore, when correlating the 2013 and 2023 maps, there is a tendency for SUHIs to decrease in

the center of São Paulo and increase in the east. However, to confirm this hypothesis, analysis of a more extensive time period would be necessary. The results are validated by the work of Oliveira *et al.* (2020), Monteiro *et al.* (2021), and Ferreira (2019), who also identified the presence of SUHIs in São Paulo and/or the São Paulo Metropolitan Region.

Conclusion

The objective of this study was to compare surface temperature and geospatial indicators for analyzing environmental variation in the city of São Paulo, Brazil, to investigate the occurrence of surface heat islands. For this purpose, the remote sensing method was used, with data from Landsat 8 over ten years.

The land cover results indicated a high urban concentration in the central areas, with vegetated remnants in the south and north of the city. Additionally, when comparing the 2013 and 2023 maps, it is evident that the urbanized area increased by 3.8%, primarily due to the loss of exposed soil. The NDBI and NDVI results showed little variability over the years, with a higher occurrence of NDBI in the central areas of the city of São Paulo, Brazil. These areas are known to be more urbanized than the perimeter regions. The areas with the highest NDVI, corresponding to parks and conservation units, showed good quality and density of vegetation. The LST results showed greater oscillations, and it was possible to notice an increase in temperature in the areas with the highest NDBI values. The average surface temperature fluctuated by approximately 9ºC, with the lowest values in 2019 and the highest in 2015. The difference in temperature between the districts with the lowest occurrence of SUHIs and those with the highest occurrence of the phenomenon was approximately 6ºC. The UTFVI values repeat the NDBI and NDVI patterns, with higher occurrences in the center and east of São Paulo, which is evident when correlating the index by district. Finally, when analyzing the SUHI maps, a contrast between locations becomes evident. Areas with better urban quality exhibit fewer occurrences of this phenomenon.

In summary, areas with high urban concentration, particularly in the central and eastern regions, exhibited increased surface temperature and recurrent surface heat island formation throughout the analyzed period, resulting in poorer UTFVI results. Peripheral regions exhibited a higher prevalence of vegetated areas and lower NDBI values. A spatial progression of SUHIs was not observed for the evaluated temporal period.

The applied method produced significant results in terms of the size of the SUHI, and it was feasible to correlate districts with low urban quality and high surface temperatures. Additionally, future works should use Level 2 images to verify potential uncertainties derived from the adopted method, as well as to analyze a longer period with data from the Landsat 5 and 7 satellites.

References

ALMEIDA, C. R.; TEODORO, A. C.; GONÇALVES, A. Study of the urban heat island (UHI) using remote sensing data/techniques: a systematic review. **Environments,** v. 8, 105, 2021.

AMORIM, M. C. de C. T. Ilhas de calor urbanas: métodos e técnicas de análise. **Revista Brasileira de Climatologia**, v. 25, 2021.

ASSOCIAÇÃO BRASILEIRA DE NORMAS TÉCNICAS. **NBR 15220**: desempenho térmico de edificações. Rio de Janeiro, 2005.

BAHI, H.; MASTOURI, H.; RADOINE, H. Review of methods for retrieving urban heat islands. **Materials Today: Proceedings**, v. 27, p. 3004–3009, 2020.

BARROS, H. R.; LOMBARDO, M. A. A ilha de calor urbana e o uso e cobertura do solo em São Paulo-SP. **Geousp – Espaço e Tempo**, v. 20, n. 1, p. 160–177, 2016.

CONGEDO, L. Semi-automatic classification plugin: a python tool for the download and processing of remote sensing images in QGIS. **Journal of Open Source Software**, v. 6, n. 64, 3172, 2021.

DORIGON, L. P.; AMORIM, M. C. C. T. Spatial modeling of an urban Brazilian heat island in a tropical continental climate. **Urban Climate**, v. 28, n. April, p. 100461, 2019.

EFFAT, H. A.; HASSAN, O. A. K. Change detection of urban heat islands and some related parameters using multi-temporal Landsat images; a case study for Cairo city, Egypt. **Urban Climate**, v. 10, n. P1, p. 171–188, 2014.

FAISAL, A. *et al.* Assessing and predicting land use/land cover, land surface temperature and urban thermal field variance index using Landsat imagery for Dhaka Metropolitan area. **Environmental Challenges**, v. 4,

2021.

FARHAN, M; YANG, Y. H.; LEE, B. G. Impact of urbanization on land surface temperature and surface urban heat Island using optical remote sensing data : a case study of Jeju Island, Republic of Korea. **Building and Environment**, v. 222, n. April, p. 109368, 2022.

FERREIRA, D. G. **A influência da superfície urbana na variação da temperatura de superfície**: uma proposta metodológica de análise. Belo Horizonte, 2021. Tese (Doutorado em Ambiente Construído e Patrimônio Sustentável) – Universidade Federal de Minas Gerais, Belo Horizonte, 2021.

FERREIRA, L. S. **Vegetação, temperatura de superfície e morfologia urbana**: um retrato da região metropolitana de São Paulo. São Paulo, 2019. Tese (Doutorado em Tecnologia da Arquitetura) – Faculdade de Arquitetura e Urbanismo, Universidade de São Paulo, São Paulo, 2019.

FERREIRA, L. S.; DUARTE, D. H. S. Exploring the relationship between urban form, land surface temperature and vegetation indices in a subtropical megacity. **Urban Climate**, v. 27, n. July 2018, p. 105–123, 2019.

FIALHO, E. S. Ilha de calor: reflexões acerca de um conceito. **Revista ACTA Geográfica**, p. 61–76, 2012.

GAMARRA, N. L. R.; CORRÊA, M. de P.; TARGINO, A. C. de L. Utilização de sensoriamento remoto em análises de albedo e temperatura de superfície em Londrina - PR: contribuições para estudos de ilha de calor urbana. **Revista Brasileira de Meteorologia**, v. 29, n. 4, p. 537–550, 2014.

GARCÍA, D.H., DÍAZ, J.A. Space–time analysis of the earth's surface temperature, surface urban heat island and urban hotspot: relationships with variation of the thermal field in Andalusia (Spain). **Urban Ecosyst**, v. 26, p. 525–546, 2023.

HALDER, B. *et al.* Investigating the relationship between land alteration and the urban heat island of Seville city using multi-temporal Landsat data. **Theoretical and Applied Climatology**, v. 150, p. 613–635, 2022.

HALDER, B.; HAGHBIN, M.; FAROOQUE, A. A. An assessment of urban expansion impacts on land transformation of rajpur-sonarpur municipality. **Knowledge-Based Engineering and Sciences**, v. 2, n. 3, p. 34–53, 2021.

KSHETRI, T. B. NDVI, NDBI and NDWI Calculation Using Landsat 7, 8. **GeoWorld**, v. 2, p. 32-34, 2018.

LOMBARDO, M. A. **Ilha de calor nas metrópoles**: o exemplo de São Paulo. São Paulo: Huci- tec/Lalekla, 1985.

MAGALHÃES, M. A.; TOSCANO, V. N.; BERGAMASCHI, R. B. Área, densidade e população: o caso de áreas urbanas e urbanizadas dos municípios do Espírito Santo. **Planejamento e Políticas Públicas (PPP), IPEA**, v. 40, jan./jun. 2013.

MONTEIRO, F. F. *et al.* Assessment of urban heat islands in Brazil based on MODIS remote sensing data. **Urban Climate**, v. 35, 2021.

NDOSSI, M. I.; AVDAN, U. Application of open source coding technologies in the production of Land Surface Temperature (LST) maps from Landsat: a PyQGIS plugin. **Remote Sensing**, v. 8, n. 5, 2016.

OKE, T. R. **Boundary layer climates**. London: Methuen & CO, 1978.

OKE, T. R. City Size and the Urban Heat Island. **Atmospheric Environment Pergamon Pres**, v. 7, p. 769–77, 1973.

OKE, T. R. Street design and urban canopy layer climate. **Energy and Buildings**, v. 11, n. 1/3, p. 103–113, 1988.

OLIVEIRA, A. B. F.; GIACAGLIA, M. E. Collaborative or adversarial production and BIM: a method for better understanding of contracting types, based on BPMN. In: CONFERENCE OF THE IBEROAMERICAN SOCIETY OF DIGITAL GRAPHICS, 22., São Carlos, 2018. **Proceedings [...]** São Carlos, 2018.

OLIVEIRA, A. P. *et al.* Assessing urban effects on the elimate of metropolitan regions of Brazil: preliminary results of the MCITY BRAZIL Project. **Exploratory Environmental Science Research**, v. 1, n. 1, p. 38–77, 2020.

PERES, L. F. *et al.* The urban heat island in Rio de Janeiro, Brazil, in the last 30 years using remote sensing

data. **International Journal of Applied Earth Observation and Geoinformation**, v. 64, n. August 2017, p. 104–116, 2018.

RAHMAN, N. *et al.* Impact of urbanization on urban heat island intensity in major districts of Bangladesh using remote sensing and geo-spatial tools. **Climate**, v. 10, n. 1, 2022.

RENARD, F. *et al.* Evaluation of the effect of urban redevelopment on surface urban heat islands. **Remote Sensing**, v. 11, n. 3, 2019.

RIBEIRO, B. M. G. **Modelagem socioambiental de resíduos sólidos em áreas urbanas degradadas**: aplicação na Bacia Mãe d'Água, Viamão. Porto Alegre, 2017. Tese (Doutorado em Planejamento Urbano e Regional) – Faculdade de Arquitetura, Universidade Federal do Rio Grande do Sul, Porto Alegre, 2017.

RODRIGUEZ-GALIANO, V. *et al.* Downscaling Landsat 7 ETM+ thermal imagery using land surface temperature and NDVI images. **International Journal of Applied Earth Observation and Geoinformation**, v. 18, n. 1, p. 515–527, 2012.

SILVA, K. A. *et al.* Analysis of vegetation dynamics using the normalized difference vegetation index (NDVI) at the archipelago of Fernando de Noronha, Pernambuco, Brazil. **Interações**, v. 21, n. 4, p. 885-901, 2020.

STREUTKER, D. R. Satellite-measured growth of the urban heat island of Houston, Texas. **Remote Sensing of Environment**, v. 85, n. 3, p. 282–289, 2003.

UNITED STATES GEOLOGICAL SURVEY. **Landsat collection 2 level-1 data.** Available: https://www.usgs.gov/landsat-missions/landsat-collection-2-level-1-data. Access: 29 mar. 2024.

UNITED STATES GEOLOGICAL SURVEY. **Landsat Missions**. Available: https://www.usgs.gov/core-science-systems/nli/landsat/landsat-8?qt-science_support_page_related_con=0#qt-science_support_page_related_con. Access em: 20 ago. 2023.

VOOGT, J. A.; OKE, T. R. Thermal remote sensing of urban climates. **Remote Sensing of Environment**, v. 86, n. 3, p. 370–384, 2003.

WANG, G. *et al.* Quantifying urban expansion and its driving forces in Chengdu, western China. **The Egyptian Journal of Remote Sensing and Space Sciences,** v. 26, 2023.

WANG, W. *et al.* Remote sensing image-based analysis of the urban heat island effect in Shenzhen, China. **Physics and Chemistry of the Earth**, v. 110, n. September 2018, p. 168–175, 2019.

WULDER, M. A. *et al.* The global Landsat archive: Status, consolidation, and direction. **Remote Sensing of Environment**, v. 185, p. 271–283, 2016.

ZHA, Y.; GAO, J.; NI, S. Use of normalized difference built-up index in automatically mapping urban areas from TM imagery. **International Journal of Remote Sensing**, v. 24, n. 3, p. 583–594, 2003.

ZHANG, Y.; ODEH, I. O. A.; HAN, C. Bi-temporal characterization of land surface temperature in relation to impervious surface area, NDVI and NDBI, using a sub-pixel image analysis. **International Journal of Applied Earth Observation and Geoinformation**, v. 11, n. 4, p. 256–264, 2009.

Acknowledgements

Financed by Fundação de Amparo à Pesquisa do Estado de São Paulo (FAPESP), process number - 2022/02552-0.

Iara Nogueira Liguori
Conceptualization, Data curation, Formal analysis, Funding acquisition, Investigation, Methodology, Software, Validation, Visualization, Writing – original draft.

Departamento de Tecnologia, Faculdade de Arquitetura e Urbanismo | Universidade de São Paulo | Rua do Lago, 876, Cidade Universitária | São Paulo – SP – Brasil | CEP 05508-080 | Tel.: (11) 3091-4538 | E-mail: iara.liguori@usp.br

Leonardo Marques Monteiro
Conceptualization, Data curation, Formal analysis, Methodology, Project administration, Resources, Supervision, Validation, Writing – review and editing.

Departamento de Tecnologia, Faculdade de Arquitetura e Urbanismo |Universidade de São Paulo | E-mail: leo4mm@usp.br

Editor: **Enedir Ghisi**

Editora convidada: **Kelen Dornelles**

Ambiente Construído
Revista da Associação Nacional de Tecnologia do Ambiente Construído
Av. Osvaldo Aranha, 99 - 3º andar, Centro
Porto Alegre – RS - Brasil
CEP 90035-190
Telefone: +55 (51) 3308-4084
www.seer.ufrgs.br/ambienteconstruido
www.scielo.br/ac
E-mail: ambienteconstruido@ufrgs.br